Available online at www.sciencedirect.com

ScienceDirect

Geochimica et Cosmochimica Acta 278 (2020) 289–304

Geochimica et Cosmochimica Acta

www.elsevier.com/locate/gca

Stable chromium isotope fractionation during magmatic differentiation: Insights from Hawaiian basalts and implications for planetary redox conditions

Ji Shen [a,b,*,1], Jiuxing Xia [c,a,1], Liping Qin [a,b], Richard W. Carlson [d], Shichun Huang [e], Rosalind T. Helz [f], Timothy D. Mock [d]

[a] CAS Key Laboratory of Crust-Mantle Materials and Environment, University of Science and Technology of China, 96 Jinzhai RD., Hefei, Anhui 230026, China

[b] CAS Center for Excellence in Comparative Planetology, China

[c] Institute of Geology and Geophysics, School of Earth Sciences, Zhejiang University, Hangzhou, Zhejiang 310027, China

[d] Department of Terrestrial Magnetism, Carnegie Institution for Science, 5241 Broad Branch Road, Washington, DC 20015, United States

[e] Department of Geoscience, University of Nevada, Las Vegas, NV 89154, United States

[f] United States Geological Survey Volcano Hazards Program VA, United States

Received 13 May 2019; accepted in revised form 1 October 2019; available online 14 October 2019

Abstract

The stable isotope compositions of chromium (Cr) are fractionated during magmatic differentiation of lunar mare basalts, which might be attributed to redox-related mineral crystallization. It has yet to be demonstrated whether magmatic differentiation fractionates Cr isotope composition of terrestrial samples. Here, we present high-precision stable Cr isotope measurements, reported as δ^{53}Cr relative to NIST SRM 979, of well-characterized Hawaiian tholeiitic basalts from Koolau, Mauna Kea and Kilauea. The studied Makapuu-stage Koolau lavas have MgO ranging from 6.58 to 21.54 wt.%, and they have homogeneous δ^{53}Cr ranging from −0.21‰ to −0.17‰. Similarly, studied Mauna Kea lavas have MgO ranging from 9.11 to 17.90 wt.%, and they also have homogeneous δ^{53}Cr ranging from −0.17‰ to −0.13‰. Some Makapuu-stage Koolau and Mauna Kea lavas experienced subaerial or submarine alteration. The homogenous δ^{53}Cr within each sample suites implies that the post-magmatic alterations have not significantly changed the Cr isotope compositions of these samples. Conversely, nine Kilauea Iki basalts have MgO ranging from 7.77 to 26.87 wt.% reflecting varying degrees of magmatic differentiation, and they show resolvable Cr isotope variations with δ^{53}Cr ranging from −0.18‰ to 0.00‰. The δ^{53}Cr values of the Kilauea Iki samples are positively correlated with indicators of magmatic differentiation such as Cr and MgO contents, and Mg# values. The most evolved samples have the lightest isotope compositions, whereas the olivine-spinel cumulates display complementary heavy isotope compositions. This fractionation is most likely generated by the crystallization and accumulation of spinel, which is dominated by Cr^{3+} and, hence, enriched in heavier Cr isotopes relative to the residual melt. At a given MgO content, Kilauea and Mauna Kea lavas, both Kea-trend volcanoes, have higher δ^{53}Cr than Makapuu-stage Koolau lavas, a Loa-trend volcano. This difference might reflect recycling of altered oceanic crusts or redox differences of their magmatic sources, with the mantle source of Makapuu-stage lavas being more reducing.

To understand the different Cr isotope fractionation behaviors of terrestrial and extraterrestrial basalts, we present a quantitative model that relates the Cr isotope compositions of basalts from the Earth, the Moon and Vesta, to the crystallization assemblage, the degree of fractional crystallization, and the $Cr^{2+}/\Sigma Cr$ ratios of minerals and melts, which are related to the

* Corresponding author at: CAS Key Laboratory of Crust-Mantle Materials and Environment, University of Science and Technology of China, 96 Jinzhai RD., Hefei, Anhui 230026, China.

E-mail address: sjlcwqqq@ustc.edu.cn (J. Shen).

[1] Authors have equal contribution.

https://doi.org/10.1016/j.gca.2019.10.003

oxygen fugacity during differentiation. The primitive Hawaiian basaltic magma for Kilauea Iki and Mauna Kea lavas is estimated to have $\delta^{53}Cr$ of −0.15‰, which is close to the average value of the BSE (−0.14‰ to −0.12‰). We further speculate that the initial lunar mantle is relatively homogeneous with BSE-like isotope composition (−0.16‰ to −0.09‰). The observed low $\delta^{53}Cr$ in lunar mafic rocks is the result of redox-dominated fractional crystallization and accumulation processes of lunar mafic magmas. These magmas might be derived from variable degrees of partial melting of the primitive lunar mantle.

Combined with previous results on the variations in Cr valences and contents in silicate melts and minerals related to oxygen fugacity, Cr concentration and isotope composition can serve as a useful oxybarometer for understanding the redox conditions of planetary differentiation and magmatic evolution.

Keywords: Cr isotope fractionation; Hawaiian basalts; Redox states; Magmatic differentiation; Planetary differentiation

1. INTRODUCTION

Chromium (Cr) is a moderately compatible and slightly siderophile element, and it can partition into both the core and the mantle during core-mantle segregation. Chromium has four stable isotopes: ^{50}Cr (4.345%), ^{52}Cr (83.789%), ^{53}Cr (9.501%) and ^{54}Cr (2.365%) (Holden et al., 2018). Chromium isotope compositions are typically expressed as permil difference in $^{53}Cr/^{52}Cr$ relative to the National Institute of Standards and Technology (NIST) Standard Reference Material 979 (SRM979), following the delta notation:

$$\delta^{53}Cr = \left[\frac{(^{53}Cr/^{52}Cr)_{Sample}}{(^{53}Cr/^{52}Cr)_{SRM979}} - 1\right] \times 1000 \quad (1)$$

Stable Cr isotope compositions have been used to constrain the formation and differentiation of the Earth and the Moon, as well as differentiated meteorites (Moynier et al., 2011; Qin et al., 2015; Bonnand et al., 2016a,b; Bonnand and Halliday, 2018; Sossi et al., 2018; Zhu et al., 2019). These studies were based on the hypothesis that the bulk-silicate Earth (BSE) has a relatively homogeneous Cr isotope composition ($\delta^{53}Cr$ of -0.12 ± 0.10‰, 2SD) (Schoenberg et al., 2008). However, Schoenberg et al. (2016) reported a small but systematic Cr isotope variability among terrestrial mantle peridotites and crustal rocks, which might be caused by mantle partial melting or crystal fractionation. Recently, a series of studies on natural samples documented resolvable Cr isotope fractionation during high temperature geological processes (Bonnand et al., 2016a; Xia et al., 2017). For example, Xia et al. (2017) observed highly variable $\delta^{53}Cr$ in mantle xenoliths from Shavaryn, Mongolia, which was attributed to kinetic isotope fractionation during melt-mantle percolation. In addition, the slightly negative correlations between $\delta^{53}Cr$ and Al_2O_3 and CaO for metasomatism- and alteration-free mantle xenoliths from Shavarynl, Haer, Hannuoba, Kimberley and Letlhakane suggested detectable Cr isotope fractionation during partial melting. The stable Cr isotope compositions of lunar mare basalts also displayed measurable variations (−0.33‰ to −0.13‰), which are positively correlated with their Mg number (Bonnand et al., 2016a). These results implied that heavy Cr isotopes preferentially partitioned into the crystallizing phases during differentiation of lunar basaltic magmas. Depending on the redox conditions, Cr could occur as Cr^{2+} and/or Cr^{3+} in minerals and melts during planetary mantle and crust formation and evolution (Berry and O'Neill, 2004; Berry et al., 2006). The behavior of Cr isotopes during mantle partial melting and basaltic magma crystal fractionation were attributed to mineral-melt fractionation, depending on the proportions of Cr^{2+} (expressed as $Cr^{2+}/\Sigma Cr$) and the Cr coordination environments in melts and minerals (Bonnand et al., 2016a; Shen et al., 2018; Xia et al., 2017).

Moynier et al. (2011) first calculated Cr isotope fractionation factors among Cr-bearing mantle minerals, and observed that spinel is isotopically heavier than olivine. Recently, Shen et al. (2018) presented a systematic study on inter-mineral Cr isotope fractionation by combining natural peridotite xenolith analyses with ionic model calculations. These results showed decreasing $^{53}Cr/^{52}Cr$ ratios in the order of spinel (Spl) > pyroxene (Py) > olivine (Ol) when in equilibrium. This could account for the previous observations of Cr isotope fractionation during both partial melting and fractional crystallization, because solid phases from both processes consist of isotopically heavy spinel (Bonnand et al., 2016a; Xia et al., 2017). Furthermore, Shen et al. (2018) predicted that the magnitude of Cr isotope fractionation is dependent on oxygen fugacity and that Cr isotope composition may be a useful tool to constrain the redox environment during magmatic processes.

Iron (Fe) isotope fractionation during mantle melting and magmatic evolution has also been shown to be depend on redox conditions (*e.g.*, Sossi et al., 2012; Dauphas et al., 2009, 2014); different redox conditions lead to distinct Fe^{3+}/Fe^{2+} proportions in minerals and melts and to differences in their corresponding Fe—O bonding force constants, resulting in melt-mineral isotope fractionation. At the planetary scale, Fe^{2+} is always dominant over Fe^{3+} in both the melt and solid phases, even under relatively oxidized conditions (*e.g.*, $Fe^{2+}/\Sigma Fe$ is ~0.84 for Earth's upper mantle or mid-ocean ridge basalts (MORBs) near the fayalite-magnetite-quartz (FMQ) buffer; Cottrell and Kelley, 2011). By contrast, $Cr^{2+}/\Sigma Cr$ values of basaltic melts and minerals (*e.g.*, olivine, pyroxene) change significantly over a large range of redox conditions. For example, $Cr^{2+}/\Sigma Cr$ values can range from ~0.45 at the nickel-nickel oxide (NNO) buffer up to ~0.90 at the IW buffer for MORB melts and crystallizing olivines at 1400 °C (Berry and O'Neill, 2004; Berry et al., 2006; Papike et al., 2016; Bell et al., 2014, 2017). Therefore, large $Cr^{2+}/\Sigma Cr$ variations in melts and minerals

make Cr isotope composition more promising than Fe isotope composition for evaluating the redox conditions during planetary-wide evolution.

Although Cr isotope has been proposed to be fractionated during lunar mafic magma evolution, oxygen fugacities of basaltic magmas from Earth [2 to 6 log units above iron-wüstite buffer (ΔIW+2 to ΔIW+6), Papike et al., 2005 and references therein] are much higher compared to those from the Moon (ΔIW−2 to ΔIW−1, Wadhwa, 2008 and references therein). Given available measurements, it is unclear whether Cr isotopes are fractionated during magma differentiation on Earth and what is the effect of oxygen fugacity. In order to investigate Cr isotope behavior during magmatic differentiation on Earth, as well as the potential effects of alteration and the incorporation of recycled crustal material in mantle-derived melts, we have analyzed twenty-one well-studied Hawaiian oceanic island basalts (OIBs) from Kilauea, Koolau and Mauna Kea.

2. SAMPLES AND GEOLOGICAL SETTING

2.1. Kilauea

Analyzed Kilauea lavas are from Kilauea Iki lava lake, located on the southeastern side of the island of Hawaii, which was formed by the eruption of the Kilauea volcano in 1959. Extensive magmatic differentiation in Kilauea Iki (Helz, 1987a) produced a wide compositional range of rocks from what is clearly a single parental magma. This makes it a classic suite to study isotope fractionation behavior during magmatic differentiation (e.g., Chen et al., 2013; Badullovich et al., 2017; Teng et al., 2007, 2008). MgO contents and Cr concentrations of the Kilauea Iki rocks vary from 2.37 to 26.87 wt.% (Helz, 1987a), and from 1.9 to 1900 ppm (Helz, 2012), respectively. Olivine crysts are common for samples with MgO contents higher than 7.0 wt.% (Helz, 1987a, b). Chromite is usually found as tiny inclusions within or at the edges of olivine crysts (Scowen et al., 1991). Olivines in samples collected from drill cores of the Kilauea Iki lava lake are geochemically zoned, suggesting that these crystals may have been in the process of re-equilibrating with the melt during slow cooling (Helz, 1987b). The quenching temperatures of the Kilauea Iki samples range from higher than 1216 °C down to 1055 °C (Helz and Thornber, 1987). The oxygen fugacity of Kilauea Iki basalts half a log unit above the FMQ buffer (Helz et al., 2017). A total of nine samples were chosen for our Cr isotope study. They include two original eruption lavas (Iki-22 and Iki-58) and 7 drill core samples from the interior of the lake, and their MgO and Cr contents range from 7.7 to 26.87 wt.%, and from 378 to 1820 ppm, respectively.

2.2. Koolau

The Koolau volcano forms the eastern part of the island of Oahu, and the Koolau caldera is located on the east coast of the island. We studied the Makapuu-stage of the Koolau volcanoes for Cr isotope composition. The source of Makapuu-stage Koolau lavas has been shown to be influenced by recycled materials as reflected by extreme radiogenic isotope compositions as well as geochemical compositions among the Hawaiian basalts (Roden et al., 1994; Eiler et al., 1996; Hauri, 1996; Lassiter and Hauri, 1998; Huang and Frey, 2005; Huang et al., 2005, 2009, 2011; Sobolev et al., 2005, 2007; Jackson et al., 2012). Thus, samples from the Koolau volcano are good candidates to evaluate the effect of recycled materials on the Cr isotope composition of Hawaiian OIBs. Frey et al. (1994) conducted a detailed geochemical and petrologic study on a suite of tholeiitic shield basalts from different sites of the Koolau volcano, showing that they were weakly altered or unaltered. Olivine phenocrysts or microphenocrysts are common for these samples, and Cr-spinel may occur as inclusions in olivine or as microphenocrysts (rare). Six tholeiitic lava samples with variable MgO contents (6.6 to 21.5 wt.%) and Cr concentrations (254 to 894 ppm) are studied. Of these, KOO17A was collected from the same lava as KOO17, but it has higher MgO content and Cr concentration (twice as much as KOO17), due to accumulation of olivine and spinel.

2.3. Mauna Kea

Mauna Kea is the tallest of the five shield volcanoes on the Big Island of Hawaii, with a height of 4205 meters above sea level. The subaerial surface of Mauna Kea is covered by postshield alkalic lavas (Frey et al., 1991). The Hawaii Scientific Drilling Project (HSDP) has been used to study the temporal geochemical variations of Mauna Kea lavas (e.g., DePaolo and Stolper, 1996; Lassiter et al., 1996; Huang and Frey, 2003; Blichert-Toft and Albarede, 2009; Rhodes et al., 2012; Silva et al., 2013). We analyzed the HSDP lavas that have been studied for intra-unit geochemical heterogeneity (Huang et al., 2016). In detail, six subaerial pahoehoe shield lavas and submarine pillow lavas, which show different degrees of alteration, were analyzed to evaluate the possible effect of post-magmatic alteration on Cr isotope compositions. Among these samples, SR0166-1.3, SR0167-1.6 and SR0168-2.9 are from unit 70, a subaerial pahoehoe flow. The other three samples are submarine pillow lavas from three different deeper units. Unit 70 samples have MgO contents ranging from 9.1 to 10.1 wt.%, and Cr contents ranging from 317 to 407 ppm. These samples have undergone alteration as revealed by their low K_2O/P_2O_5 (~0.5) and high Ba/Rb ratios (75.7 to 110.6) (Table 1, Huang et al., 2016). The deeper samples (SR0756-1.0, SR0808-8.8 and SR0823-10.8) display relatively higher MgO (12.3 to 17.9 wt.%) and Cr contents (641 to 963 ppm), with high K_2O/P_2O_5 (0.45 to 1.81) and low Ba/Rb ratios (13.7 to 61.5) (Table 1).

3. ANALYTICAL METHODS

Chromium column chemistry and isotope analyses were carried out at the Department of Terrestrial Magnetism (DTM) of the Carnegie Institution for Science. Procedures for sample digestion, chemical separation and instrumental analyses are similar to previous studies (Trinquier et al.,

Table 1
Chromium isotope compositions of the Hawaiian basalts analyzed in this study together with other geochemical data.

Sample	δ^{53}Cr (‰)	±2SD ‰	Cr (ppm)	SiO_2 (wt.%)	Al_2O_3 (wt.%)	Fe(t) (wt.%)	MgO (wt.%)	LOI (wt.%)	Ba/Rb	Sr/Nb
Kilauea Iki										
Iki-22	−0.11	0.04	1318	46.68	9.52	13.01	19.52	<0.5	11.07	18
Iki-58	−0.17	0.04	378	49.91	12.69	12.40	8.08	<0.5	9.64	16
KI67-3-6.8	−0.14	0.04	1630	44.63	7.58	13.36	25.83	<0.5	11.06	15
KI75-1-39.0	−0.11	0.04	752	48.39	11.78	12.66	12.46	<0.5	-	-
KI75-1-121.5	−0.18	0.04	479	50.00	13.46	11.72	7.77	<0.5	10.61	20
KI79-3-150.4	−0.16	0.04	1108	48.44	11.72	11.72	13.51	<0.5	13.71	20
KI81-1-169.9	0.00	0.04	1290	43.71	6.10	16.44	26.87	<0.5	10.85	13
KI81-1-210.0	−0.09	0.04	1700	44.87	7.64	13.59	24.53	<0.5	10.17	17
KI81-1-239.9	−0.08	0.04	1820	44.21	6.92	14.24	26.55	<0.5	8.15	19
Mean	−0.12	0.10								
Koolau										
KOO-10	−0.17	0.04	652	50.82	12.73	11.55	13.57	<1	21.98	45
KOO-17	−0.21	0.04	395	52.09	13.05	11.17	10.71	<1	14.91	45
KOO-17a	−0.17	0.04	894	46.57	9.13	12.69	21.54	<1	-	44
KOO-19	−0.20	0.04	261	53.07	14.11	10.86	8.86	<1	13.80	42
KM1	−0.20	0.05	846	51.02	11.61	11.83	6.58	<1	22.50	58
OH25	−0.17	0.04	254	50.26	15.64	11.88	7.04	<1	103.75	46
Mean	−0.19	0.03								
Mauna Kea										
SR0166-1.3	−0.16	0.04	407	46.64	13.83	13.96	10.14	2.16	135.00	22
SR0167-1.6	−0.15	0.04	328	46.83	13.88	14.16	9.17	2.09	198.33	21
SR0168-2.9	−0.14	0.04	317	47.32	13.49	13.75	9.11	1	232.50	22
SR0756-1.0	−0.16	0.04	963	46.90	10.05	12.79	17.90	0.38	17.58	23
SR0808-8.8	−0.13	0.04	647	47.21	11.89	13.24	12.86	1.14	15.00	22
SR0823-10.8	−0.17	0.04	641	47.54	12.06	13.20	12.30	4.78	162.22	20
Mean	−0.15	0.03								

Major element contents, Cr concentrations, Ba/Rb and Sr/Nb ratios are from Helz (1987a, 2012), Frey et al., (1994) and Huang et al. (2016), LOI values of the Kilauea Iki and Koolau samples are assessed by the given H_2O and CO_2 concentrations.

2008; Qin et al., 2010; Shen et al., 2015; Xia et al., 2017). A brief description is given in the following.

3.1. Sample digestion and chemical separation

Whole-rock powders were digested by either an oxidative alkaline fusion method for spinel-bearing samples or by conventional acid digestion (HF-HCl-HNO_3) for non-spinel-bearing samples. Detailed information about the digestion method and the Cr purification is given in Qin et al. (2010) and Xia et al. (2017). Following the sample digestion, an appropriate amount of the ^{50}Cr-^{54}Cr double spike was added to a sample aliquot containing ~1 μg Cr, as determined by ICP-MS before starting the column chemistry, to achieve a sample to spike ratio of 1:1. Samples digested by the oxidative alkaline fusion method were processed following a three-step cation exchange protocol (Bio-Rad AG50W X8 resin) to separate Cr from the matrix. Samples dissolved by conventional acid digestion methods were purified using a two-step ion exchange protocol. The final Cr elution was dried down three or more times in concentrated HNO_3. The recovery of Cr through the columns is about 70–80%, and the total procedural blank is <10 ng, which is negligible compared with the total amount of loaded Cr (1000 ng).

3.2. Mass spectrometry

Chromium isotope analyses were performed on a Thermo Finnigan Triton multi-collector thermal ionization mass spectrometer (TIMS) at DTM, following the procedures described in Qin et al. (2010) and Shen et al. (2015). Purified Cr was loaded onto single out-gassed Re filaments, and ionized between 1250 and 1380 °C for the isotope measurements to avoid possible interferences at higher ionization temperatures (*e.g.,* Ti, V, Fe, Qin et al., 2010). $^{50}Cr^+$, $^{52}Cr^+$, $^{53}Cr^+$ and $^{54}Cr^+$ were collected in static mode on Faraday detectors L2, Axial, H1 and H2, respectively. To assess potential interferences from $^{50}Ti^+$, $^{50}V^+$ and $^{54}Fe^+$, the intensities of $^{49}Ti^+$, $^{51}V^+$ and $^{56}Fe^+$ were simultaneously determined on Faraday cups L3, L1 and H4, respectively. All Faraday cups were connected to 10^{11} Ω resistors, and the typical beam intensity of $^{52}Cr^+$ was ~5 V. The samples and standards were generally analyzed once during one analytical session. Each measurement consisted of 14 blocks of 30 cycles, with an 8 s integration time. The long-term reproducibility of the NIST SRM 979 standard on δ^{53}Cr is ± 0.04‰ (n = 26, 2SD). Results for the reference rock standards (PCC-1, BHVO-1 and BIR-1) have been reported in our previous work (Xia et al., 2017), which were consistent with results determined using MC-ICP-MS

(Bonnand et al., 2016a; Schoenberg et al., 2008). The reported uncertainty of the samples analyzed here is the long-term (2SD) reproducibility of the NIST SRM979 standard (~0.04‰), which is larger than either the typical two standard error of the sample measurement (0.01 to 0.04‰), or the external error (2SD) of the NIST SRM979 standard analyzed during the same sessions as the samples (0.02 to 0.04‰).

4. RESULTS

The measured $\delta^{53}Cr$ for the twenty-one Hawaiian basalt samples vary from -0.21 ± 0.04‰ to 0.00 ± 0.04‰ (Table 1). Koolau and Mauna Kea lavas have limited Cr isotope composition variations, with average $\delta^{53}Cr$ values of -0.19 ± 0.03‰ (2SD) and -0.15 ± 0.03‰ (2SD), respectively. In contrast, Kilauea Iki lavas show considerable Cr isotope variations, with $\delta^{53}Cr$ ranging from 0.00 $\pm$ 0.04‰ (sample KI81-1-169.9, with the highest MgO content of 26.87 wt.%) to -0.18 ± 0.04‰ (sample KI75-1-121.5, with the lowest MgO content of 7.73 wt.%). Student *t*-tests reveal that the average $\delta^{53}Cr$ value of the Koolau samples is significantly lower than the mean value of the Mauna Kea samples, as well as the mean value of the Kilauea Iki samples (-0.12 ± 0.10‰, 2SD), while the difference between Mauna Kea and Kilauea Iki lavas is insignificant. As shown in Fig. 1, Cr isotope compositions of these Hawaiian samples show positive correlations with whole-rock MgO and FeO(tot) contents and negative correlations with SiO_2 contents.

5. DISCUSSION

In this section, we first discuss the effects of post-magmatic alteration and incorporation of recycled materials into the mantle source on the Cr isotope compositions of the Hawaiian basalts. Then, we assess the behavior of Cr isotopes during magmatic differentiation, including the relationship between Cr isotope fractionation and redox conditions. Finally, we discuss the implications of Cr isotope fractionation related to the evolution of terrestrial planets associated with redox conditions.

5.1. Effects of post-magmatic alteration and incorporation of recycled material on Cr isotope compositions

After eruption, some Hawaiian OIBs experienced different types and degrees of post-magmatic alterations, including interactions with seawater during submarine alteration and with fresh water during subaerial alteration (Huang et al., 2016). Both processes could lead to leaching of K and Rb from basalts into fluids; thus, high Ba/Rb and low K_2O/P_2O_5 ratios are often taken as alteration indicators (Frey et al., 1994; Huang et al., 2016). Additionally, the LOI (loss on ignition) value is another index of aqueous ($\pm CO_2$) alteration. As shown in Fig. 2b-d, $\delta^{53}Cr$ values of the Mauna Kea and Koolau basalts do not change significantly with increasing degree of alteration, indicating that post-magmatic alterations have not significantly modified $\delta^{53}Cr$ at the level of our analytical uncertainty. These

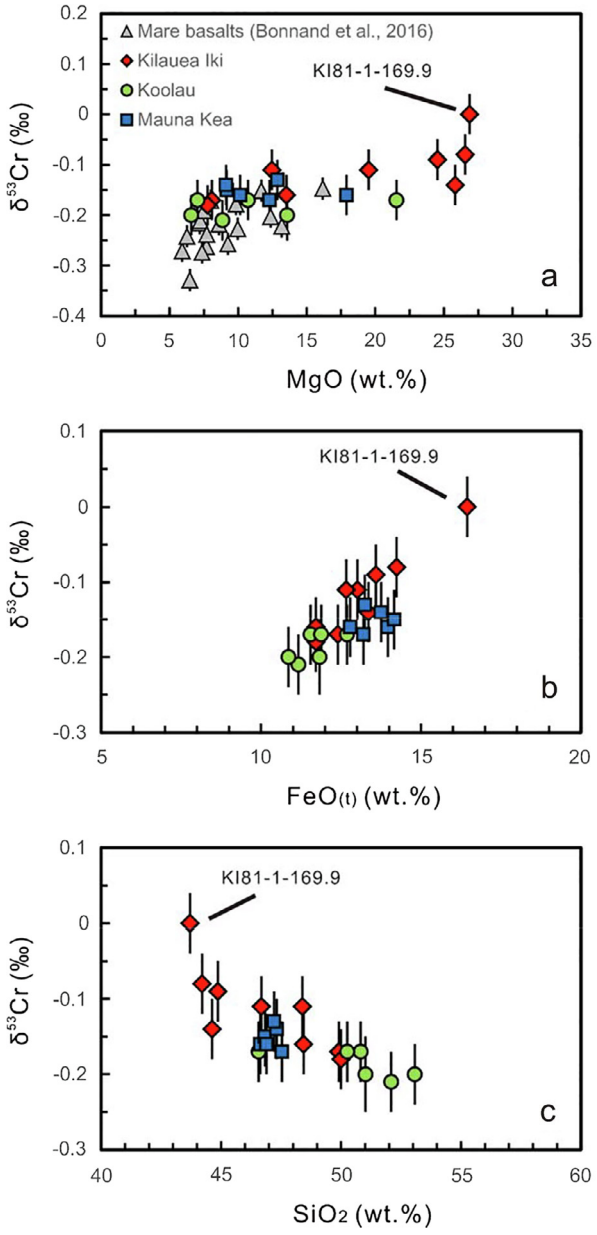

Fig. 1. Chromium isotope compositions ($\delta^{53}Cr$) versus MgO (a), $FeO_{(t)}$ (b) and SiO_2 (c) in Hawaiian oceanic island basalts (OIBs) analyzed in this study. One sample (KI81-1-169.9) deviates from the trends in (a)-(c) and is related to the formation of segregation veins, causing this sample to be enriched in interstitial melt and depleted in augite and spinel (Helz, 1980, 2012). Major element concentrations for Hawaiian OIBs are from Frey et al. (1994), Helz (1987a,b, 2012) and Huang et al. (2016). Grey triangles in (a) represent the lunar mare basalts from Bonnand et al. (2016). The error bars for the Hawaiian OIBs in this and all subsequent figures represent 2SD uncertainties, as defined in the main text.

results are consistent with the limited Cr isotope variation of mildly altered oceanic basalts from ODP Site 504 (Wang et al., 2016). Therefore, the slightly lower $\delta^{53}Cr$ in ODP Hole 504B mafic lavas (-0.23‰ to -0.17‰, Wang et al., 2016) and Makapuu-stage Koolau lavas (-0.21‰ to -0.17‰, this study), compared to estimated BSE values

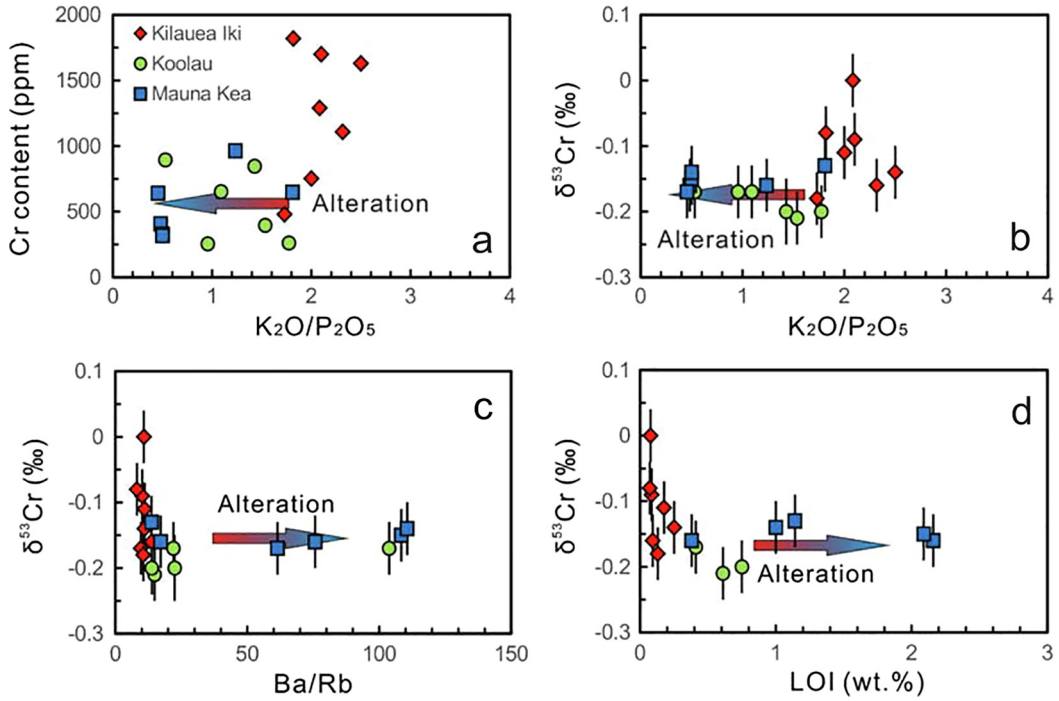

Fig. 2. Plot (a) displays the relationship between Cr content and the post-magmatic alteration indicator K_2O/P_2O_5. Plots (b) to (d) show the Cr isotope variations versus K_2O/P_2O_5 ratios (b), Ba/Rb ratios (c), and LOI values (d) for Hawaiian OIB whole-rocks during post-magmatic alteration. Major and trace element concentrations for Hawaiian OIBs are from Frey et al. (1994), Helz (1987a,b, 2012) and Huang et al. (2016).

(−0.21‰ to −0.02‰, Schoenberg et al., 2008), are unlikely a result of alteration. This might be attributed to the fact that there is no significant loss of Cr during post-magmatic alteration due to the low mobility of mineral-forming Cr^{3+} (Fig. 2a). Therefore, we propose that the major cause of Cr isotope variability of the investigated OIBs may be either from source heterogeneity or from mass-dependent isotope fractionation during magmatic differentiation.

Previous works have proposed that the post-magmatic alterations could lead to loss of SiO_2 and increases of $FeO_{(t)}$ (Frey et al., 1994; Rhodes and Vollinger, 2004; Huang et al., 2016), thus, the trends in both diagrams of $\delta^{53}Cr$ vs. $FeO_{(t)}$ and SiO_2 may not represent fractionation during magmatic evolution, especially for the Koolau samples. On the other hand, the Koolau samples with MgO of 6.58 wt.% to 21.54 wt.% have $\delta^{53}Cr$ values varying within a limited range of −0.21‰ to −0.17‰, which are indistinguishable within the error bars (0.04‰, 2SD). Thus, the slightly light Cr isotope compositions of Koolau samples relative to Kilauea and Mauna Kea samples should reflects different compositions or redox conditions of their mantle sources, rather than isotope fractionations during magmatic differentiation.

Recycling of oceanic basalts and carbonates has been used to explain the anomalous compositions of Sr, Nd, Pb and Ca isotopes of Koolau shield lavas (Lassiter and Hauri, 1998; Huang et al., 2005, 2009, 2011). The Koolau samples display lower $\delta^{53}Cr$ values than the rest Hawaiian samples with similar MgO contents. One possible interpretation is that their mantle source is slightly isotopically lighter than the mantle sources of the Kilauea and Mauna Kea. We take Sr/Nb ratios as an indicator of incorporation of marine carbonates and altered oceanic crusts (Plank and Langmuir, 1998; Bach et al., 2003; Huang et al., 2011). A slightly negative correlation between Sr/Nb and $\delta^{53}Cr$ values in Fig. 3 suggests that some recycled material with light isotope compositions might have lowered the $\delta^{53}Cr$ of the Koolau samples. To further assess the effects of recycled materials, two mixing curves were modeled between a typical Hawaiian basaltic magma (e.g., Sr/Nb = 20, $\delta^{53}Cr = -0.15‰$) and recycled sedimentary carbonates or altered oceanic basalts. The high positive $\delta^{53}Cr$ measured by Bonnand et al. (2013) rules out a sedimentary carbonate component in the source of these lavas as a cause for the slightly lighter isotope compositions of the Koolau samples (Fig. 3). Although altered oceanic basaltic crust was proposed to be isotopically indistinguishable from unaltered basaltic crust, as well as BSE (Wang et al., 2016), all but one of the hydrothermally altered oceanic basalts from Ocean Drilling Program (ODP) Hole 504B display slightly lighter Cr isotope features (−0.23 to −0.17‰). The simple two-end-member mass balance calculation, which could account for the Koolau sample data (Fig. 3), implies that their Cr isotope features might be generated by incorporation of altered oceanic crust materials like those from ODP 504B.

Alternatively, the small offset in Cr isotope compositions between the Koolau (Makapuu-stage) and Kilauea + Mauna Kea samples could also be generated by Cr isotope fractionation during partial melting under different redox conditions of their sources, which has been

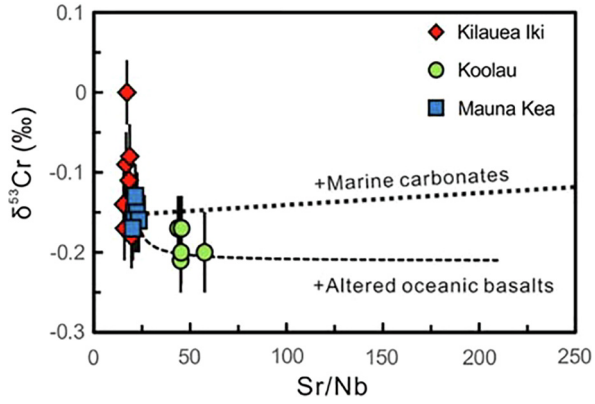

Fig. 3. The diagram presents the potential effects of recycling sedimentary carbonates and altered oceanic crusts into the Hawaiian plume on whole-rock Cr isotope compositions of Hawaiian OIBs. The element and Cr isotope compositions of marine carbonates are from Plank and Langmuir (1998) and Bonnand et al. (2013), while the altered oceanic crust data are from Bach et al. (2003) and Wang et al. (2016).

documented in our recent work (Shen et al., 2018). Lighter Cr isotope compositions require that the source of Koolau is more reducing (Fig. 4b). This speculation is consistent with calculation results that the oxygen fugacities of Koolau samples (~ΔFMQ−1) were lower than those of other Hawaiian lavas (ΔFMQ−0.8 to ΔFMQ+0.5) by using the olivine-melt equilibrium method (McCann and Barton, 2005). Furthermore, Teng et al. (2013) observed that the source of the Makapuu-stage Koolau lavas has a slightly lighter Fe isotope composition than those of the Kilauea samples, which could also be the result of isotope fractionation under more reducing conditions (Fig. 4a, Dauphas et al., 2009).

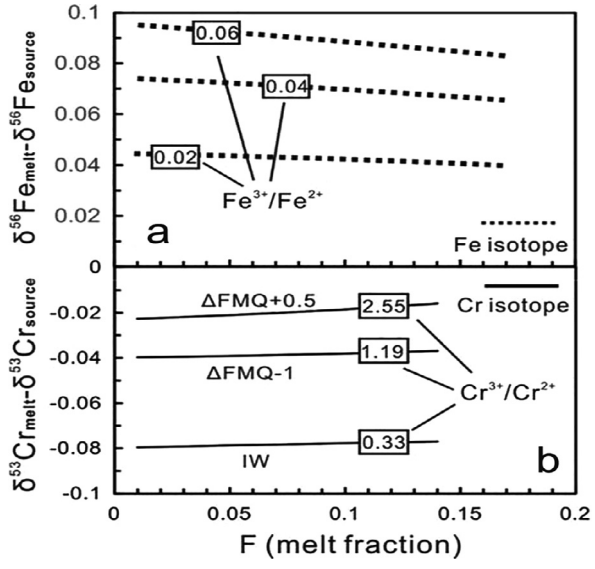

Fig. 4. Plots give calculated Fe (a) and Cr (b) isotope fractionations between melts and residuals as a function of melt fraction (F) associated with oxygen fugacities during partial melting of mantle peridotite. The numbers on the curves represent Fe^{3+}/Fe^{2+} and Cr^{3+}/Cr^{2+} ratios of initial mantle peridotites, respectively. The calculated curves are based on Dauphas et al. (2009) for Fe isotope, and Shen et al. (2018) for Cr isotope. Notably, the calculated model for Cr isotope is modified by using new constrains on Cr^{2+}/Cr^{3+} ratios of pyroxenes based on partition coefficients of Cr^{2+} and Cr^{3+} between pyroxenes and melts (Mallmann and O'Neill, 2009), thus the calculated curve is different from that in Shen et al. (2018).

5.2. Chromium isotope fractionation during differentiation of basaltic magma

Kilauea Iki lava lake was filled with a single lava flow that experienced limited crustal contamination or late-stage alteration. The large chemical variations observed in the samples from this area were attributed to magmatic evolution processes (Helz and Thornber, 1987; Helz, 1987a,b, 2012; Teng et al., 2007). Two primary magmatic processes account for most of the observed compositional variation. These include: olivine + spinel accumulation for samples with MgO > ~11.5 wt.%, and a crystallization sequence of olivine (+spinel), augite, plagioclase and Fe-Ti oxide phases for samples with MgO from ~11.5 wt.% to < ~3 wt.% (Fig. 5a, Helz and Thornber, 1987; Helz, 1987a,b, 2012; Zhang et al., 2018). For example, olivine and spinel are proposed to be the first crystallization phases from basaltic magma from MgO of ~11.5 wt.% to ~7.5 wt.% (Roeder et al., 2001, 2006; Zhang et al., 2018), while augite and plagioclase begin to crystallize at MgO of ~7.5 wt.% and ~6.7 wt.%, respectively (Helz and Thornber, 1987; Helz, 2012; Zhang et al., 2018). The Fe-Ti oxide minerals finally crystallize at MgO contents lower than 5.5 wt.% (Helz and Thornber, 1987; Helz, 2012). The investigated Kilauea Iki lavas have MgO contents of 7.7 to 26.87 wt.%, which predominantly record cotectic olivine and spinel crystallization and accumulation (Roeder et al., 2006; Helz, 2012). This inference is supported by the linear relationships between Cr concentration and MgO ($R^2 = 0.87$, Fig. 5a) and SiO_2 contents ($R^2 = 0.80$, Fig. 5b). The Cr isotope compositions of Kilauea Iki basalts show small but systematic variations accompanying fractional crystallization and accumulations of these minerals. The most magnesian samples, with the highest proportion of olivine and spinel, tend to have the heaviest Cr isotope compositions, whereas the two most differentiated samples display the lightest $\delta^{53}Cr$ values (Fig. 5a, b). The $\delta^{53}Cr$ values are moderately correlated with MgO ($R^2 = 0.56$, Fig. 5a) and SiO_2 ($R^2 = 0.63$, Fig. 5b), documenting that magmatic differentiation fractionates Cr isotopes. This correlation may reflect fractional crystallization (for samples with MgO < ~11.5 wt.%) or accumulation of olivine and spinel (for samples with MgO > ~11.5 wt.%), because spinels have higher Cr contents and heavier Cr isotope compositions relative to the melt (Bonnand et al., 2016a; Shen et al., 2018; Xia et al., 2017). In the following, both kinetic and equilibrium processes are evaluated.

5.2.1. Kinetic process

Before assessing equilibrium isotope fractionation during fractional crystallization and accumulation, kinetic diffusion of Cr isotopes was first evaluated in Kilauea Iki

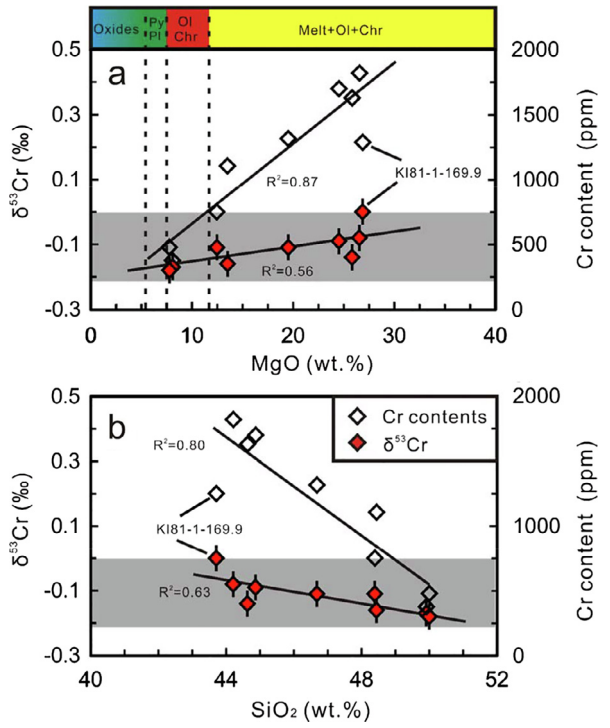

Fig. 5. Plot (a) shows the $\delta^{53}Cr$ and Cr concentration versus the degree of magma differentiation as represented by the MgO content for the Kilauea Iki samples. Seven samples with MgO > ~11.5 wt.% represent mixtures of melts and crystallized olivine + Cr-spinel (chromite), whereas the samples with MgO < ~11.5 wt.% reflect fractional crystallization of olivine + spinel, followed by augite, plagioclase and Fe-Ti oxides (Helz, 1987a, b; Zhang et al., 2018). The two samples with MgO of 7.77 and 8.08 wt.%, represent residual melt after fractional crystallization of olivine + Cr-spinel (chromite). Similarly, plot (b) presents correlations of $\delta^{53}Cr$ and Cr concentration with SiO_2 contents for Kilauea Iki samples. The grey band represents the $\delta^{53}Cr$ range of BSE (−0.124‰±0.104, 2SD) from Schoenberg et al. (2008) in both plots (a) and (b). Mineral abbreviations: Ol = olivine, Chr = chromite, Py = pyroxene, Pl = plagioclase.

samples. Three potential diffusion processes might lead to isotope composition variations for these samples, including thermal diffusion, chemical diffusion and redox-induced diffusion, during fractional crystallization and subsequent re-equilibration between crystallized phases and the residual melt.

During fractional crystallization, there was a large thermal gradient (65 °C/m) in the vertical direction for the Kilauea Iki lake lava (Helz and Thornber, 1987). According to the crystallization history of Kilauea Iki lavas using MELTS, the lavas with higher MgO contents generally have higher temperatures than those of low MgO lavas (Zhang et al., 2018). Despite the lack of direct experimental determination of Cr isotope behavior during thermal diffusion, Cr isotope fractionation behavior might be similar to that of Fe isotope fractionation during thermal diffusion, based on their similar diffusing species and thermal diffusion isotope sensitivities (Li and Liu, 2015). Thus, one can expect that light Cr isotopes will tend to be enriched in the higher-temperature region (samples with high MgO contents), and thermal diffusion should generate a trend of increasingly heavy Cr from the high MgO lavas to low MgO ones. However, this expectation is inconsistent with our observations, and thus could not be the cause for the observed Cr isotope variations.

Chemical diffusion during re-equilibration of olivines with evolved melts was used to explain large $\delta^{26}Mg$ and $\delta^{56}Fe$ variations and the negative correlation between them in Kilauea Iki olivine phenocrysts (Teng et al., 2011). Compared to olivines, most Cr-spinel occurred as inclusions in olivines. Consequently, they were shielded by olivine, and re-equilibrium with host magma may not happen. Furthermore, even though Cr diffusion has taken place (e.g., across host olivines, Scowen et al., 1991), considerably lower diffusion coefficient (1–2 orders) of Cr than Fe and Mg in olivines at 1150 °C (Dohmen et al., 2007; Ito and Ganguly, 2006; Posner et al., 2016) imply that information on early isotope equilibrium fractionation could be preserved. A simple diffusion model calculation documents that Cr isotope variations of spinel within olivine, during 21 years of magmatic cooling, determined by Mg-Fe isotope diffusion (Teng et al., 2011), is very limited (<+0.02‰). Therefore, we propose that the Cr isotope variations of the investigated Kilauea Iki lava lake samples may record early isotope equilibrium fractionations, instead of fractionations caused by chemical diffusion during re-equilibrium process.

Excluding thermal and chemical diffusion, Teng et al. (2008) proposed that kinetic isotope fractionation caused by different redox states might be an alternative interpretation for whole-rock Fe isotope variations, and a lack of Mg isotope fractionation. Their argument was based on the positive correlation between $Fe^{3+}/\Sigma Fe$ and $\delta^{56}Fe$ (Fig. 6a). During oxidation and reduction processes, the isotope behavior of Cr is similar to Fe, thus, the same trend is expect for $Fe^{3+}/\Sigma Fe$ and $\delta^{53}Cr$. However, the negative correlations between $Fe^{3+}/\Sigma Fe$ and $\delta^{53}Cr$ (Fig. 6a), and between $\delta^{56}Fe$ and $\delta^{53}Cr$ (Fig. 6b), rule out this possibility. Instead, the negative correlations between $Fe^{3+}/\Sigma Fe$ and $\delta^{53}Cr$ could be interpreted as reflecting equilibrium mineral-melt fractionation where olivine hosts most of the Fe (almost cFe^{2+}), and spinel hosts most of the Cr and is characterized by heavy Cr isotope compositions (Shen et al., 2018). The positive correlation between $\delta^{53}Cr$ and $\delta^{56}Fe$ may reflect that both equilibrium and kinetic isotope fractionations are controlled by redox conditions, e.g., Fe isotope fractionation during olivine crystallization and re-equilibrium with melt is suggested to be governed by distribution of Fe^{3+} and Fe^{2+} between the mineral and the residual melt (Teng et al., 2008; Dauphas et al., 2017), and Cr isotope fractionation is governed by distribution of Cr^{2+} and Cr^{3+} (Shen et al., 2018).

5.2.2. Equilibrium Cr isotope fractionation

Determination of the Cr isotope fractionation factors between basaltic melts and minerals (spinel and olivine) for Kilauea Iki basalts is difficult. Our recent work, however, allows us to make a reasonable estimation of the equilibrium isotope effect during spinel and olivine crystallization and accumulation (Shen et al., 2018). Generally,

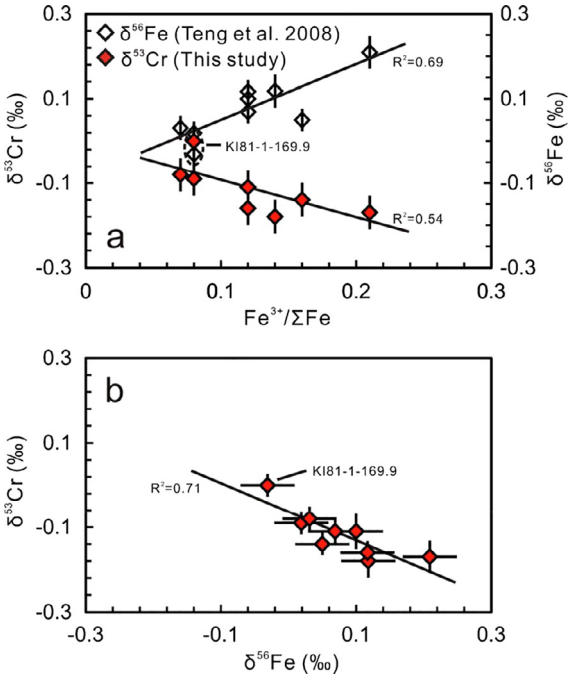

Fig. 6. (a) Plot of $Fe^{3+}/\Sigma Fe$ versus Cr and Fe isotope compositions for Kilauea Iki samples; (b) The correlation of $\delta^{53}Cr$ and $\delta^{56}Fe$ for Kilauea Iki samples. The $Fe^{3+}/\Sigma Fe$ values and the Fe isotope data are from Teng et al. (2008).

heavy Cr isotopes concentrate in the phase with low coordination number and high valence state, similar to isotope systems of other polyvalent elements, such as Fe (*e.g.*, Dauphas et al., 2014; Macris et al., 2015; Sossi and O'Neill, 2017). In terrestrial basaltic melts and minerals, divalent and trivalent Cr are the predominant species, with Cr^{2+}/Cr^{3+} being strongly dependent on the redox environment of the magmatic system (Berry and O'Neill, 2004; Berry et al., 2006; Bell et al., 2014, 2017; Papike et al., 2016;). Berry and O'Neill (2004) and Berry et al. (2006) presented detailed experiments and synchrotron X-ray absorption near edge structure (XANES) analyses to conclusively document that $Cr^{2+}/\Sigma Cr$ values of basaltic melts can vary from ~1 to 0 depending on f_{O2} of the melt. Similar experiments to determine the Cr valance were made on olivines crystallized from basaltic melts. The results showed that the $Cr^{2+}/\Sigma Cr$ value of olivine is identical to that of its equilibrium magma (Bell et al., 2014, 2017), which is consistent with the indistinguishable partition coefficients of Cr^{2+} and Cr^{3+} between olivine and melt (Mallmann and O'Neill, 2009; Bell et al., 2017). Trivalent Cr in both melt and olivine is in 6-coordination (Papike et al., 2005; O'Neill and Berry, 2006), and thus no isotopic fractionation between Cr^{3+} in olivine and melt is expected. However, the lower coordination number of Cr^{2+} (4-coordination, Miletich et al., 1999; O'Neill and Berry, 2006) in melts relative to olivine (6-coordination, Papike et al., 2005; Shen et al., 2018) leads to an enrichment of heavy Cr isotopes in the melt Cr^{2+} relative to olivine. In contrast, Cr in spinel is always in the +3 valence based on stoichiometry and XANES measurements (O'Neill and Navrotsky, 1984; Shen et al., 2018). Considering that Cr^{3+} in spinel always occupies 6-coordinated sites (Papike et al., 2005), the stronger 6-coordinated Cr^{3+}—O bond strength in spinel relative to 4-coordinated Cr^{2+}—O bond in melt (*e.g.*, K value in Table 2) causes spinel to be isotopically heavier than the equilibrium melt. The degree of isotope fractionation depends on the $Cr^{2+}/\Sigma Cr$ value of the melt, which is related to oxygen fugacity (Shen et al., 2018). Observations of isotopically heavier spinels in natural peridotites relative to the BSE are consistent with these expectations (Farkaš et al., 2013; Shen et al., 2015). Chromium is highly compatible in chromite ($D_{chromite/melt}$ = 500–1000, Roeder et al., 2006), and slightly incompatible in olivine ($D_{olivine/melt}$ = ~0.85, Mallmann and O'Neill, 2009). Natural and experimental observations revealed a cotectic ratio of olivine to spinel/chromite of ~100 during the crystallization of basaltic melts (Roeder et al., 2006); thus, spinel should be the predominant Cr host (>85 wt.%) during crystallization, and dominate Cr isotope fractionation between melts and crystallized phases. Therefore, equilibrium isotope fractionations between minerals (spinel and olivine) and melts can account for the enrichment of isotopically heavy Cr isotopes in cumulates with high Cr contents and complementary melts characterized by light Cr isotopes and low Cr contents as seen in the investigated Kilauea Iki basalts.

5.3 A. quantitative estimation of the effect of oxygen fugacity on equilibrium Cr isotope fractionation

5.3.1. Model calculations

As discussed above, Cr isotope variation of Kilauea Iki basalts can be attributed to equilibrium fractionation during fractional crystallization and accumulation of olivine and spinel. Similar to Kilauea Iki, Cr isotopic variations in lunar mare basalts can also be attributed to fractional crystallization of olivine, spinel, and clinopyroxene. Lunar mafic rocks have lighter Cr isotope compositions relative to the Kilauea Iki basalts and the BSE, but the cause remains controversial (Bonnand et al., 2016a; Sossi et al., 2018). In this section, we will quantitatively assess to which extent oxygen fugacity can affect the Cr isotope fractionation during basaltic magma evolution. Such an assessment could help better understand stable Cr isotope fractionation in terrestrial and extraterrestrial samples, as well as explore potential implications for tracing redox condition variation during planetary differentiation.

We calculate the Cr isotope compositions of magmas and crystallizing phases (*e.g.*, olivine, pyroxene, spinel) as functions of oxygen fugacity using the ionic model of Shen et al. (2018). The proportion of Cr^{2+} (expressed as $Cr^{2+}/\Sigma Cr$) of the primitive basaltic melts for the Earth, Moon and other planets are quantitatively calculated according to the experimental results of Berry et al. (2006), and the $Cr^{2+}/\Sigma Cr$ ratios of the crystallizing minerals equilibrated with the melts are calculated using the partition coefficients of Cr^{2+} and Cr^{3+} between minerals and melts (Mallmann and O'Neill, 2009). We discussed in detail the Cr^{2+} and Cr^{3+} coordination in minerals (Shen et al., 2018). The Cr^{2+} coordination numbers are 6 in olivine and ~7 in pyroxene, whereas Cr^{3+} is 6 coordinated in oli-

Table 2
Parameters for Cr isotope fractionation of basaltic melt-mineral system during fractional crystallization.

	f_{O2}[a]	Initial melt		$Cr^{2+}/\Sigma Cr$[c]				$K_{f,Cr-O}$ (N/m)[d]				Fractionation factor (‰, 1150 °C)		
		Cr content (ppm)[b]	$\delta^{53}Cr$ (‰)	Melt	Ol	Cpx	Spl	Melt	Ol	Cpx	Spl	$\Delta^{53}Cr_{Ol\text{-}Melt}$	$\Delta^{53}Cr_{Cpx\text{-}Melt}$	$\Delta^{53}Cr_{Spl\text{-}Melt}$
Hawaii, Earth	ΔFMQ±1	700	−0.15	0.55	0.55	0.05	0	1677.3	1349	1854.2	1917.7	−0.086	0.046	0.063
HEDs, Vesta	IW-1 to IW	3600	−0.15	0.9	0.9	0.3	0	1503.1	1055.5	1521.5	1917.7	−0.118	0.005	0.109
Mare, Moon	IW-2 to IW-1	4000	−0.17 to −0.23	0.95	0.95	0.47	0	1476.7	1017.2	1316.2	1917.7	−0.121	−0.042	0.116

[a] The oxygen fugacities are from Gerlach (1993), Helz et al. (2017), Herd (2008), McCann and Barton (2004) and Wadhwa (2008).
[b] Cr contents in initial basaltic melts are estimated by Cr solubility in spinel-saturated melts (Hanson and Jones, 1998; Roeder and Reynolds, 1991) and Cr contents in natural samples with MgO of ~11 wt.% (Bonnand et al., 2016a; Helz, 2012; Schoenberg et al., 2016).
[c] $Cr^{2+}/\Sigma Cr$ values of melts are estimated according to the experimental results from Berry et al. (2006) at a given oxygen fugacity. $Cr^{2+}/\Sigma Cr$ values of olivine and clinopyroxene minerals are calculated by Cr^{2+} and Cr^{3+} partition coefficients (Mallmann and O'Neill, 2009), *e.g.*, $D_{Ol\text{-}Melt}$ of 0.85 for both Cr^{2+} and Cr^{3+}, $D_{Cpx\text{-}Melt}$ of 0.587 and 12.6 for Cr^{2+} and Cr^{3+}, respectively.
[d] The corresponding force constants ($K_{f,Cr\text{-}O}$) for melt and minerals according to Eq. (1) from Shen et al. (2018) and Young et al. (2015).

vine, pyroxene and spinel. Furthermore, Cr^{3+} in the basaltic magma strongly favors regular octahedral coordination (6-coordinated), whereas Cr^{2+} typically is tetragonally coordinated or in a square planar geometry (4-coordinated, Miletich et al., 1999; O'Neill and Berry, 2006). Therefore, the average force constants of Cr—O bonding in individual minerals and melts can be written as (Shen et al., 2018):

$$K_{f,ij} = \frac{z_i z_j e^2 (1-n)}{4\pi\varepsilon_0 r_{ij}^3} \tag{2}$$

where z_i and z_j are the valences of cations and anions, e is the charge of an electron, ε_0 is the electric constant (vacuum permittivity), r_{ij} is the equilibrium inter-ionic distance between cation i and anion j, and n is the Born-Mayer constant for the repulsion term (empirically equal to 12) (Young et al., 2015; Shen et al., 2018). Equilibrium mineral-melt Cr isotope fractionation factors at a given temperature (T in K) are expressed as (Shen et al., 2018):

$$\Delta^{53}\mathrm{Cr}_{a-b} = \delta^{53}Cr_a - \delta^{53}Cr_b \approx 10^3 ln\alpha_{a-b}^{53/52} = \frac{10^3}{24}\left(\frac{h}{k_b T}\right)^2\left(\frac{1}{m_{52}} - \frac{1}{m_{53}}\right)\left[\frac{K_{f,a}}{4\pi^2} - \frac{K_{f,b}}{4\pi^2}\right], \tag{3}$$

where m_{52} and m_{53} are the atomic masses of ^{52}Cr and ^{53}Cr, respectively, k_b is Boltzmann's constant, h is Planck's constant, and $K_{f,a}$ and $K_{f,b}$ are the average force constants for phases a (*e.g.*, minerals) and b (*e.g.*, melts), respectively.

We take Cr^{2+} and Cr^{3+} as two individual species to determine the degree of isotope fractionation during fractional crystallization following Sossi and O'Neill (2017) and Shen et al. (2018). Individual partition coefficients between the minerals and the basaltic magma, based on spinel-facies peridotites from Mallmann and O'Neill (2009), are used in the fractional crystallization model. Detailed parameters are given in Table 2. We assume that the partitioning for ^{52}Cr, the 84% isotope, is equivalent to the bulk partition coefficient of elemental Cr summed over each isotope:

$$D_{a-b}^{^{52}Cr} = \sum_i D_{a-b}^{Cr}. \tag{4}$$

Thus, the partition coefficient for ^{53}Cr can be expressed by combining Eqs. (3) and (4):

$$D_{a-b}^{^{53}Cr} = \left(D_{a-b}^{^{52}Cr}\right) e^{\left(\frac{\Delta^{53}\mathrm{Cr}_{a-b}}{10^3}\right)} \tag{5}$$

With respect to Raleigh fractional crystallization of a basaltic magma, Cr concentrations in the residual melt and the crystalline phase can be expressed as:

$$\frac{C_m}{C_o} = F^{(D_0-1)} \tag{6}$$

and

$$\frac{C_s}{C_o} = \frac{1 - F^{D_0}}{1 - F} \tag{7}$$

where C_0, C_m and $C_s$are the Cr concentrations in the bulk system, melt and solid, respectively. D_0 is the Cr partition

coefficient in the crystalline phase relative to the melt, and F is the residual melt fraction relative to the primary melt.

The concentrations of each of the isotopes can be expressed as:

$$\frac{(^{53}C_{Cr})_s/(^{53}C_{Cr})_m}{(^{52}C_{Cr})_s/(^{52}C_{Cr})_m} = \frac{D^{53}_{s-m}}{D^{52}_{s-m}} = \alpha^{53/52}_{s-m} \quad (8)$$

where the ratio of ^{53}Cr to ^{52}Cr in the crystalline phase relative to the melt could represent the ratio of their partition coefficients or the fractionation factor (Sossi and O'Neill, 2017). In Eq. (8), the partition coefficients for both ^{53}Cr and ^{52}Cr are the sum of those of different crystallized mineral assemblages, expressed as:

$$D^j_{s-m} = \sum_i s_i D^j_{s_i-m} \quad (9)$$

where s_i represents the mass fraction of different minerals in solids, and $D^j_{s_i-m}$ is the corresponding partition coefficient of isotope j (*e.g.,* ^{52}Cr or ^{53}Cr) between different mineral phase (i) and the melt. Thus, the concentrations of ^{52}Cr and ^{53}Cr in the melt and the crystalline phase are calculated by substituting Eqs. (8) and (9) into Eqs. (6) and (7):

$$\frac{C^j_m}{C^j_0} = F^{(\sum_i s_i D^j_{s_i-m}-1)} \quad (10)$$

for the melt, and

$$\frac{C^j_s}{C^j_0} = \frac{1-F^{(\sum_i s_i D^j_{s_i-m})}}{1-F} \quad (11)$$

for the crystalline phase. The resulting isotope compositions of the melt and the crystalline phase can be calculated as:

$$\delta^{53}Cr_m = \delta^{53}Cr_0 + 10^3 \ln\left(\frac{C^{53}_m/C^{53}_0}{C^{52}_m/C^{52}_0}\right) \quad (12)$$

and

$$\delta^{53}Cr_s = \delta^{53}Cr_0 + 10^3 \ln\left(\frac{C^{53}_s/C^{53}_0}{C^{52}_s/C^{52}_0}\right) \quad (13)$$

respectively.

5.3.2. Calculation results and implications

The effects of redox conditions on Cr isotope fractionation were assessed by modelling the evolution of basaltic magmas on the Earth and Moon, as well as other planets. The oxygen fugacities of Hawaiian OIB (Kilauea Iki and Mauna Kea) and lunar (ultra)mafic magmas were ΔFMQ ± 1 and ΔIW−2 to ΔIW−1, respectively, corresponding to $Cr^{2+}/\Sigma Cr$ of ~0.55 and ~0.95 in the Hawaiian primary magma and lunar primary magma (Berry et al., 2006). According to the partition coefficients (Mallmann and O'Neill, 2009), the crystallized minerals in equilibrium with the melt should have $Cr^{2+}/\Sigma Cr$ values of 0.55 for olivine and 0.05 for clinopyroxene at Hawaii, and 0.95 for olivine and 0.47 for clinopyroxene under lunar mantle conditions. In both scenarios, Cr in spinel is +3 charged, based on stoichiometry calculations (O'Neill and Navrotsky, 1984) and X-ray absorption near edge spectroscopy (XANES) measurements of natural spinel from terrestrial mantle peridotites and lunar mare basalts (Sutton et al., 1993; Shen et al., 2018). The temperature at the depth for fractional crystallization of olivine and spinel from primary basaltic melts is taken to be ~1150 °C (Helz and Thornber, 1987; Hallis, 2010; Bonnand et al., 2016a). The force constants (K) for the melts and minerals are calculated using Eq. (2) under this temperature, and are presented in Table 2. The Hawaiian primary melt has a K_{Melt} value of 1677.3 N/m, while the force constants of fractionally crystallized olivine, clinopyroxene and spinel in equilibrium with the melt are $K_{Ol} = 1349.0$ N/m, $K_{Cpx} = 1854.2$ N/m, and $K_{Spl} = 1917.7$ N/m, respectively. This results in $\Delta^{53}Cr_{\text{Ol-Melt}} = -0.086‰$, $\Delta^{53}Cr_{\text{Cpx-Melt}} = +0.046‰$, and $\Delta^{53}Cr_{\text{Spl-Melt}} = +0.063‰$ at 1150 °C. Here, we adopt an initial basaltic magma with δ^{53}Cr of −0.15‰ to best match the observed Kilauea Iki data. According to the proposed Rayleigh fractionation crystallization model, with a cotectic ratio of ~100 for crystallized olivine and spinel (Roeder et al., 2006), the observed Cr isotope variations of the Kilauea Iki basalts are in good agreement with the calculated fractional crystallization and accumulation curves (Fig. 7). Utilizing $K^{Fe-Mg}_{D_{Ol-Melt}} = 0.28$ (Helz et al., 2017), two evolved Kilauea Iki basalts (Iki-58 and KI75-1-121.5) have the crystallization proportion (5.1–7.2%) of olivine and spinel, consistent with the calculated crystallization proportion for Cr isotope fractionation (5–8%, Fig. 7).

Among the Kilauea Iki samples, KI81-1-169.9 deviates from the calculated curve, and displays low Cr content and heavy Cr isotope composition compared to the sample with similar MgO and SiO_2 contents (Figs. 5a, b and 7). Its high δ^{53}Cr value most likely not reflect equilibrium isotope fractionation of simply fractional crystallization or accumulation processes, as it would require an unrealistic $\Delta^{53}Cr_{\text{Spl-Melt}}$ value of ~0.2‰, even higher than that under a very reduced condition (like the Moon, Table 2). Furthermore, this sample has been proposed to be related to the formation of the ferrodiabasic segregation veins by filter-pressing of internal differentiated melt into fractures within crystal mush zones (Helz, 1980, 2012; Helz et al., 1989). Relative to the normal matrix rocks, this sample is enriched in interstitial melt and depleted in augite and plagioclase, and has a lower Cr content (Helz, 2012). Equilibrium fractionation caused by augite fractionation cannot explain its heavy Cr isotope feature, because $\Delta^{53}Cr_{\text{Cpx-Melt}}$ is positive (Table 2). Here we propose a multiple differentiation processes to explain its Cr and Fe isotope signatures. In the hottest core recovered from the lava lake, there was still some late-crystallized spinel in the groundmass which are not included by olivines, in addition to early-stage crystallizing spinels within olivine grains. These late-stage spinels should have lighter Cr isotope and heavier Fe isotope compositions than those crystallized earlier within olivines, because late-stage melts trend to have lower δ^{53}Cr and higher δ^{56}Fe values than initial magma melts (this work and Teng et al., 2008). As temperature decreases, all late-stage spinels which are not protected by olivines are dissolved into augites when they crystallize, and no spinels would survive outside olivine by 1140 °C (Helz et al.,

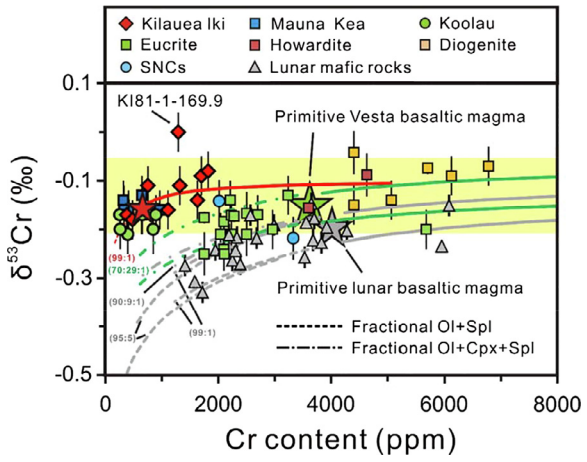

Fig. 7. Model calculations on stable Cr isotope fractionation during magmatic differentiation for Kilauea Iki samples from this study, lunar mafic rocks from Bonnand et al. (2016a) and Sossi et al. (2018), HEDs and SNCs from Bonnand et al. (2016b), Schoenberg et al. (2016) and Zhu et al. (2019). The modeling parameters are given in Table 2, and the calculations follow the method described in the main text (Shen et al., 2018; Sossi and O'Neill, 2017). The stars in different colors are the estimated compositions of primitive basaltic magmas for Earth, Moon and Vesta. The dotted lines represent fractionation curves for residual melts after fractional crystallization of different mineral assemblages, while the numbers in parentheses are the volumetric proportions of crystallized mineral assemblages, *e.g.,* 99:1 represents factional crystallization of 99% olivine + 1% spinel by volume, and 90:9:1 represents fractional crystallization of 90% olivine + 9% clinopyroxene + 1% spinel by volume. The solid red and grey lines represent the mixing curves between initial melts and crystallized mineral assemblages (99% olivine + 1% spinel by volume) for terrestrial and lunar cumulates, and the green solid lines represent the mixing curves between initial melts and crystallized mineral assemblages (70% olivine + 29% clinopyroxene + 1% by volume) for Vesta diogenites. The yellow area represents the stable Cr isotope composition range of the BSE (Schoenberg et al., 2008). (For interpretation of the references to colour in this figure legend, the reader is referred to the web version of this article.)

1989). Considering that almost all Cr and part of Fe from the crystallizing augites were taken up from the late-stage spinel (Helz et al., 1989; Helz, 2012), the Cr and Fe that were lost with the augites would have the signature of the late-stage spinel, i.e., low δ^{53}Cr and higher δ^{56}Fe, which leads to the distinctive isotope features of vertical olivine- and vein- rich bodies in Kilauea Iki.

According to the model calculations, the δ^{53}Cr value of the initial magma for Hawaiian OIBs (Kilauea Iki + Mauna Kea) is estimated to be −0.15‰ based on data-fitting, which is close to the average value of the BSE (−0.12‰ to −0.14‰, Schoenberg et al., 2008, 2016; Xia et al., 2017). Similar approaches are employed to assess the published lunar mafic rock data from Bonnand et al. (2016a) and Sossi et al. (2018). Compared with terrestrial basaltic magmas, the lower lunar oxygen fugacity environment leads to significantly higher Cr concentrations of lunar mafic melts and the associated minerals (olivine, pyroxene), consistent with the higher Cr solubilities in reduced spinel-saturated melts and associated minerals (Roeder and Reynolds, 1991; Hanson and Jones, 1998). Furthermore, the reduced melts and minerals have higher $Cr^{2+}/\Sigma Cr$ values (Berry and O'Neill, 2004; Berry et al., 2006; Papike et al., 2016). For a mare basaltic magma with $Cr^{2+}/\Sigma Cr$ of ~0.95 and an f_{O2} of ΔIW-2 to ΔIW-1, the K_{Melt} value is 1476.7 N/m, which translates into larger equilibrium Cr isotope fractionation in $\Delta^{53}Cr_{Spl\text{-}Melt}$ of +0.116‰ between spinel and the melt at 1150 °C (Table 2). The equilibrium Cr isotope fractionation between olivine and melt is also larger ($\Delta^{53}Cr_{Ol\text{-}Melt} = -0.121‰$) compared to −0.086‰ for the Hawaiian magma (Table 2). Thus, the crystallization of either spinel or olivine at lower oxygen fugacity generates larger isotope variations in δ^{53}Cr for both crystallizing and residual phases. During lunar magmatic evolution, spinel is also a common crystallized phase at the early stage associated with olivine crystallization (Hallis, 2010 and references therein), and the assemblage of olivine + spinel should be predominant during early fractional crystallization of lunar mafic magmas. The different crystallization portions of spinel to olivine may have insignificantly effects on Cr isotope compositions of melts, as a small amount of spinel crystals can already control the budget of elemental Cr and its isotope composition in the crystallization phases (Fig. 7). This result supports that our model is suitable for the lunar basalts, in which the model abundances of spinel vary from ~0.1 vol.% to 2.83 vol.% (Hallis, 2010). With respect to some low-Mg lunar mafic rocks, which have undergone additional clinopyroxene crystallization, the Cr isotope fractionation between the solid and the melt phases is slightly lowered. This is due to the fact that clinopyroxenes have a high Cr partition coefficient, but a $\Delta^{53}Cr_{Cpx\text{-}Melt}$ of ~0 (Table 2). Most data fall on modeled lines for fractional crystallization of relatively homogeneous initial lunar basaltic magmas with δ^{53}Cr of −0.23‰ to −0.17‰ (Fig. 7), which is slightly lower than the average value for the BSE (−0.12‰ to −0.14‰, Schoenberg et al., 2008, 2016; Xia et al., 2017), and the estimated value of the initial Hawaiian OIB magma (−0.15‰).

Does this δ^{53}Cr difference in inferred terrestrial (Hawaii) and lunar primitive magmas reflect a δ^{53}Cr difference in the terrestrial mantle and lunar mantle? We propose that the difference in Cr isotope compositions between lunar and terrestrial primitive magmas could reflect fractionation during partial melting, since lower oxygen fugacity trends to generate isotopically lighter partial melts (Fig. 4b). For example, partial melting of a spinel-facies peridotite under the ΔIW buffer at 1300 °C could fractionate the melts by −0.07‰ to −0.08‰ in δ^{53}Cr (Fig. 4b). Lower degrees of melting to generate the lunar mare basalts (e.g., ~1%, Hallis, 2010) would lead to larger isotope fractionations, thus isotopically lighter melts. According to the estimated partial melting degrees given by Hallis (2010), the Cr isotope composition of the primitive lunar mantle peridotite source before partial melting is estimated to be in a range of −0.16‰ to −0.09‰ by utilizing the non-modal partial melting model proposed by Shen et al. (2018), in line with that of BSE. Therefore, we attribute the light Cr isotope features of the lunar mafic rocks to redox-dominated frac-

tional crystallization and accumulation processes, as well as variable melting degrees of the primitive lunar mantle with BSE-like Cr isotope compositions. This paper thus presents an alternative interpretation to the idea of an oxidizing volatile (CrO_2) loss process leading to an enrichment of ^{52}Cr in lunar magma melts (Sossi et al., 2018).

The conclusion that redox conditions dominate equilibrium Cr isotope fractionation during magmatic processes can provide a potential tool for understanding the redox conditions of magma genesis for differentiated silicate meteorites. Because spinel-saturated basaltic melts are characterized by lower Cr contents and Cr^{2+}/Cr^{3+} values under more oxidized conditions than in the lunar mantle (Roeder and Reynolds, 1991), mafic rocks from differentiated meteorites that formed under oxygen fugacity conditions of ~IW to the ~FMQ buffer may vary between the regions of two fractionation curves defined by terrestrial and lunar mafic rocks (Fig. 7). For instance, the stable Cr isotope compositions of a series of Howardite, Eucrites and Diogenites (HEDs) have been reported by Bonnand et al. (2016b), Schoenberg et al. (2016) and Zhu et al. (2019). According to our model, most of the evolved eucrites can also be interpreted by fractional crystallization of isotopically heavier olivine + clinopyroxenes + spinel from a terrestrial mantle-like magma source under ΔIW-1 to IW buffer conditions (Fig. 7). The estimated Cr isotope composition of the initial magma yields −0.19‰ to −0.13‰, which is between the lunar basaltic magma source and the BSE, in consistent with our prediction. This result also supports that the observed Cr isotope variations of the HEDs were a result of equilibrium fractionation during magma differentiation under the relatively reducing condition of Vesta mantle. Apart from one sample (Shalka), other diogenites could represent the accumulation of isotopically heavy mineral phases (*e.g.*, spinel; Fowler et al., 1994; Bowman et al., 1999), whereas two howardites (Kapoeta and Luotolax) may reflect brecciated mixtures of eucrites and diogenites in different proportions (Fig. 7, Mittlefehldt et al., 2013). So far, Cr isotope data were reported for only two SNC meteorites (Nakhla and Chassigy) by Bonnand et al. (2016b) and Schoenberg et al. (2016). Although the two samples plot within the area between Earth and Moon, further work is warranted to assess whether magma evolution under relatively oxidized Martian conditions (ΔIW−1 to ΔIW+2.5, Wadhwa, 2008 and references therein) or source heterogeneity best explains the position of the Martian data in Fig. 7.

6. CONCLUSIONS

We present high-precision stable Cr isotope compositions of twenty-one Hawaiian basalts that show considerable variation in $\delta^{53}Cr$ of −0.21‰ to 0.00‰. The samples from Koolau and Mauna Kea have relatively homogenous Cr isotope compositions, whereas the $\delta^{53}Cr$ values of the basalts from Kilauea Iki are positively correlated with whole-rock Cr concentrations, MgO and FeO(t) contents, and are negatively correlated with SiO_2, Al_2O_3 and CaO abundances. Taken together, this implies that Cr isotopes are fractionated during basaltic magma evolution. The Cr isotope fractionation for basalts from Kilauea Iki reflect mixing of isotopically heavy spinel + olivine cumulates with residual melt. Furthermore, our data are combined with those for lunar mafic rocks, HEDs and SNCs to show that the degree of fractionation is related to planetary mantle redox conditions. A quantitative model that relates the Cr isotope composition of basalts to the crystallizing assemblage, the degree of fractional crystallization and the $Cr^{2+}/\Sigma Cr$ ratios (dominated by redox conditions) is presented. The model is able to explain the observed Cr isotope variations in the Hawaiian basalts, as well as those observed in other planetary bodies (Moon, Vesta and Mars). Because Cr isotope fractionation during the evolution of basaltic magmas is controlled by redox conditions, Cr isotopes can be used as an oxybarometer to understand the oxygen fugacity conditions during planetary differentiation and magmatic evolution.

ACKNOWLEDGMENT

We thank Mary Horan (Department of Terrestrial Magnetism (DTM) of the Carnegie Institution for Science) for her guidance in the geochemistry lab. We thank Fangzhen Teng (Department of Earth and Space Sciences, University of Washington) for providing us the samples of Kilauea Iki and Koolau, and Xuefang Li for discussions about Cr isotope behavior during thermal diffusion. This work is supported by Strategic Priority Research Program (B) of Chinese Academy of Sciences (Grant No. XDB18000000), the National Nature Science Foundation of China (41625013, 41721002, 41730216 to Liping Qin, and 41973004, 41673006 to Ji Shen), and the Fundamental Research Funds for the Central Universities of China (WK2080000102).

REFERENCES

Bach W., Peucker-Ehrenbrink B., Hart S. R. and Blusztajn J. S. (2003) Geochemistry of hydrothermally altered oceanic crust: DSDP/ODP Hole 504B–Implications for seawater-crust exchange budgets and Sr-and Pb-isotopic evolution of the mantle. Geochem. Geophys. Geosyst..

Badullovich N., Moynier F., Creech J., Teng F. and Sossi P. (2017) Tin isotopic fractionation during igneous differentiation and Earth's mantle composition. *Geochem. Persp. Lett.* **5**, 24–28.

Bell A., Burger P., Le L., Shearer C., Papike J., Sutton S., Newville M. and Jones J. (2014) XANES Measurements of Cr Valence in Olivine and their Applications to Planetary Basalts. *Am. Mineral.* **99**, 1404–1412.

Bell A. S., Shearer C., Burger P., Ren M., Newville M. and Lanzirotti A. (2017) Quantifying and correcting the effects of anisotropy in XANES measurements of chromium valence in olivine: Implications for a new olivine oxybarometer. *Am. Mineral.* **102**, 1165–1172.

Berry A. J. and O'Neill H. S. C. (2004) A XANES determination of the oxidation state of chromium in silicate glasses. *Am. Mineral.* **89**, 790–798.

Berry A. J., O'Neill H. S. C., Scott D. R., Foran G. J. and Shelley J. (2006) The effect of composition on Cr2+/Cr3+ in silicate melts. *Am. Mineral.* **91**, 1901–1908.

Blichert-Toft J. and Albarède F. (2009) Mixing of isotopic heterogeneities in the Mauna Kea plume conduit. *Earth Planet. Sci. Lett.* **282**, 190–200.

Bonnand P. and Halliday A. (2018) Oxidized conditions in iron meteorite parent bodies. *Nat. Geosci.* **11**, 401.

Bonnand P., James R. H., Parkinson I. J., Connelly D. P. and Fairchild I. J. (2013) The chromium isotopic composition of seawater and marine carbonates. *Earth Planet. Sci. Lett.* **382**, 10–20.

Bonnand P., Parkinson I. J. and Anand M. (2016a) Mass dependent fractionation of stable chromium isotopes in mare basalts: Implications for the formation and the differentiation of the Moon. *Geochim. Cosmochim. Acta* **175**, 208–221.

Bonnand P., Williams H., Parkinson I., Wood B. and Halliday A. (2016b) Stable chromium isotopic composition of meteorites and metal–silicate experiments: Implications for fractionation during core formation. *Earth Planet. Sci. Lett.* **435**, 14–21.

Bowman L. E., Papike J. J. and Spilde M. N. (1999) Diogenites as asteroidal cumulates: Insights from spinel chemistry. *Am. Mineral.* **84**, 1020–1026.

Chen H., Savage P. S., Teng F.-Z., Helz R. T. and Moynier F. (2013) Zinc isotope fractionation during magmatic differentiation and the isotopic composition of the bulk Earth. *Earth Planet. Sci. Lett.* **369**, 34–42.

Cottrell E. and Kelley K. A. (2011) The oxidation state of Fe in MORB glasses and the oxygen fugacity of the upper mantle. *Earth Planet. Sci. Lett.* **305**, 270–282.

Dauphas N., Craddock P. R., Asimow P. D., Bennett V. C., Nutman A. P. and Ohnenstetter D. (2009) Iron isotopes may reveal the redox conditions of mantle melting from Archean to Present. *Earth Planet. Sci. Lett.* **288**, 255–267.

Dauphas N., John S. G. and Rouxel O. (2017) Iron isotope systematics. *Rev. Mineral. Geochem.* **82**(1), 415–510.

Dauphas N., Roskosz M., Alp E., Neuville D., Hu M., Sio C., Tissot F., Zhao J., Tissandier L. and Médard E. (2014) Magma redox and structural controls on iron isotope variations in Earth's mantle and crust. *Earth Planet. Sci. Lett.* **398**, 127–140.

DePaolo D. and Stolper E. (1996) Models of Hawaiian volcano growth and plume structure: Implications of results from the Hawaii Scientific Drilling Project. *J. Geophys. Res. Solid Earth* **101**, 11643–11654.

Dohmen R., Becker H.-W. and Chakraborty S. (2007) Fe–Mg diffusion in olivine I: experimental determination between 700 and 1,200 C as a function of composition, crystal orientation and oxygen fugacity. *Phys. Chem. Miner.* **34**, 389–407.

Eiler J. M., Farley K. A., Valley J. W., Hofmann A. W. and Stolper E. M. (1996) Oxygen isotope constraints on the sources of Hawaiian volcanism. *Earth Planet. Sci. Lett.* **144**, 453–467.

Farkaš J., Chrastný V., Novák M., Čadkova E., Pašava J., Chakrabarti R., Jacobsen S. B., Ackerman L. and Bullen T. D. (2013) Chromium isotope variations (δ53/52Cr) in mantle-derived sources and their weathering products: Implications for environmental studies and the evolution of δ53/52Cr in the Earth's mantle over geologic time. *Geochim. Cosmochim. Acta* **123**, 74–92.

Fowler G., Papike J., Spilde M. and Shearer C. (1994) Diogenites as asteroidal cumulates: Insights from orthopyroxene major and minor element chemistry. *Geochim. Cosmochim. Acta* **58**, 3921–3929.

Frey F., Garcia M. and Roden M. (1994) Geochemical characteristics of Koolau Volcano: Implications of intershield geochemical differences among Hawaiian volcanoes. *Geochim. Cosmochim. Acta* **58**, 1441–1462.

Frey F., Garcia M., Wise W., Kennedy A., Gurriet P. and Albarede F. (1991) The evolution of Mauna Kea volcano, Hawaii: petrogenesis of tholeiitic and alkalic basalts. *J. Geophys. Res. Solid Earth* **96**, 14347–14375.

Gerlach T. (1993) Oxygen buffering of Kilauea volcanic gases and the oxygen fugacity of Kilauea basalt. *Geochim. Cosmochim. Acta* **57**, 795–814.

Hallis L. (2010) The Geology of the Moon: Geochemistry and Petrology of Lunar Basalts. The Open University.

Hanson B. and Jones J. H. (1998) The systematics of Cr3+ and Cr2 + partitioning between olivine and liquid in the presence of spinel. *Am. Mineral.* **83**, 669–684.

Hauri E. H. (1996) Major-element variability in the Hawaiian mantle plume. *Nature* **382**, 415.

Helz R. (1980) Crystallization history of Kilauea Iki lava lake as seen in drill core recovered in 1967–1979. *Bull. Volcanologique* **43**, 675–701.

Helz R. (1987a) Character of olivines in lavas of the 1959 eruption of Kilauea Volcano and its bearing on eruption dynamics. *U.S. Geol. Surv. Prof. Pap.* **1350**, 691–722.

Helz R. T. (1987b) Differentiation behavior of Kilauea Iki lava lake, Kilauea Volcano, Hawaii: an overview of past and current work. *Magmatic Processes: Physicochem. Principles* **1**, 241–258.

Helz R. T. (2012) Trace-element analyses of core samples from the 1967-1988 drillings of Kilauea Iki lava lake, Hawaii. US Department of the Interior, US Geological Survey.

Helz R. T., Cottrell E., Brounce M. N. and Kelley K. A. (2017) Olivine-Melt relationships and syneruptive redox variations in the 1959 Eruption of Kīlauea volcano as revealed by XANES. *Bull. Volcanol. Geothermal Res.* **333-334**, 1–14.

Helz R. T., Kirschenbaum H. and Marinenko J. W. (1989) Diapiric transfer of melt in Kilauea Iki lava lake, Hawaii: a quick, efficient process of igneous differentiation. *Geol. Soc. Am. Bull.* **101**, 578–594.

Helz R. T. and Thornber C. R. (1987) Geothermometry of Kilauea Iki lava lake, Hawaii. *Bull. Volcanol.* **49**, 651–668.

Herd C. D. (2008) Basalts as probes of planetary interior redox state. *Rev. Mineral. Geochem.* **68**, 527–553.

Holden N. E., Coplen T. B., Bohlke J. K., Tarbox L. V., Benefield J., Laeter J. R., Mahaffy P. G., O'Connor G., Roth E., Tepper D. H., Walczyk T., Wieser M. E. and Yoneda S. (2018) IUPAC Periodic Table of the Elements and Isotopes (IPTEI) for the Education Community (IUPAC Technical Report). *Pure Appl. Chem.* **90**(12), 1833–2092.

Huang S., Abouchami W., Blichert-Toft J., Clague D. A., Cousens B. L., Frey F. A. and Humayun M. (2009) Ancient carbonate sedimentary signature in the Hawaiian plume: evidence from Mahukona volcano,Hawaii. *Geochem. Geophys. Geosyst.* **10**(8).

Huang S., Farkaš J. and Jacobsen S. B. (2011) Stable calcium isotopic compositions of Hawaiian shield lavas: evidence for recycling of ancient marine carbonates into the mantle. *Geochim. Cosmochim. Acta* **75**, 4987–4997.

Huang S. and Frey F. (2003) Trace element abundances of Mauna Kea basalt from phase 2 of the Hawaii Scientific Drilling Project: Petrogenetic implications of correlations with major element content and isotopic ratios. *Geochem. Geophys. Geosyst.*, 4.

Huang S. and Frey F. A. (2005) Recycled oceanic crust in the Hawaiian Plume: evidence from temporal geochemical variations within the Koolau Shield. *Contrib. Miner. Petrol.* **149**, 556–575.

Huang S., Frey F. A., Blichert-Toft J., Fodor R., Bauer G. R. and Xu G. (2005) Enriched components in the Hawaiian plume: evidence from Kahoolawe Volcano, Hawaii. *Geochem. Geophys. Geosyst.* **6**(11).

Huang S., Vollinger M. J., Frey F. A., Rhodes J. M. and Zhang Q. (2016) Compositional variation within thick (> 10m) flow units of Mauna Kea Volcano cored by the Hawaii Scientific Drilling Project. *Geochim. Cosmochim. Acta* **185**, 182–197.

Ito M. and Ganguly J. (2006) Diffusion kinetics of Cr in olivine and 53Mn–53Cr thermochronology of early solar system objects. *Geochim. Cosmochim. Acta* **70**, 799–809.

Jackson M. G., Weis D. and Huang S. (2012) Major element variations in Hawaiian shield lavas: Source features and perspectives from global ocean island basalt (OIB) systematics. *Geochem. Geophys. Geosyst.* **13**(9).

Lassiter J., DePaolo D. and Tatsumoto M. (1996) Isotopic evolution of Mauna Kea volcano: Results from the initial phase of the Hawaii Scientific Drilling Project. *J. Geophys. Res. Solid Earth* **101**, 11769–11780.

Lassiter J. and Hauri E. (1998) Osmium-isotope variations in Hawaiian lavas: evidence for recycled oceanic lithosphere in the Hawaiian plume. *Earth Planet. Sci. Lett.* **164**, 483–496.

Li X. and Liu Y. (2015) A theoretical model of isotopic fractionation by thermal diffusion and its implementation on silicate melts. *Geochim. Cosmochim. Acta* **154**, 18–27.

Macris C. A., Manning C. E. and Young E. D. (2015) Crystal chemical constraints on inter-mineral Fe isotope fractionation and implications for Fe isotope disequilibrium in San Carlos mantle xenoliths. *Geochim. Cosmochim. Acta* **154**, 168–185.

Mallmann G. and O'neill H. S. C. (2009) The crystal/melt partitioning of V during mantle melting as a function of oxygen fugacity compared with some other elements (Al, P, Ca, Sc, Ti, Cr, Fe, Ga, Y, Zr and Nb). *J. Petrol.* **50**, 1765–1794.

McCann, V., Barton, M., 2004. Oxygen Fugacities of Lavas From Iceland and Implications for Mantle Redox States, AGU Spring Meeting Abstracts.

McCann, V., Barton, M., 2005. Olivine-Melt Equilibrium and the Oxygen Fugacities of Lavas from Hawaii, AGU Spring Meeting Abstracts.

Miletich R., Nowak M., Seifert F., Angel R. and Brandstätter G. (1999) High-pressure crystal chemistry of chromous orthosilicate, Cr2SiO4. A single-crystal X-ray diffraction and electronic absorption spectroscopy study. *Phys. Chem. Miner.* **26**, 446–459.

Mittlefehldt D. W., Herrin J. S., Quinn J. E., Mertzman S. A., Cartwright J. A., Mertzman K. R. and Peng Z. X. (2013) Composition and petrology of HED polymict breccias: The regolith of (4) Vesta. *Meteori Planet Sci.* **48**, 2105–2134.

Moynier F., Yin Q.-Z. and Schauble E. (2011) Isotopic evidence of Cr partitioning into Earth's core. *Science* **331**, 1417–1420.

O'Neill H. S. C. and Berry A. J. (2006) Activity coefficients at low dilution of CrO, NiO and CoO in melts in the system CaO–MgO–Al2O3–SiO2 at 1400 C: using the thermodynamic behaviour of transition metal oxides in silicate melts to probe their structure. *Chem. Geol.* **231**, 77–89.

O'Neill H. S. C. and Navrotsky A. (1984) Cation distributions and thermodynamic properties of binary spinel solid solutions. *Am. Mineral.* **69**, 733–753.

Papike J., Karner J. and Shearer C. (2005) Comparative planetary mineralogy: Valence state partitioning of Cr, Fe, Ti, and V among crystallographic sites in olivine, pyroxene, and spinel from planetary basalts. *Am. Mineral.* **90**, 277–290.

Papike J. J., Simon S. B., Burger P. V., Bell A. S., Shearer C. K. and Karner J. M. (2016) Chromium, vanadium, and titanium valence systematics in Solar System pyroxene as a recorder of oxygen fugacity, planetary provenance, and processes. *Am. Mineral.* **101**, 907–918.

Plank T. and Langmuir C. H. (1998) The chemical composition of subducting sediment and its consequences for the crust and mantle. *Chem. Geol.* **145**, 325–394.

Posner E. S., Ganguly J. and Hervig R. (2016) Diffusion kinetics of Cr in spinel: Experimental studies and implications for 53Mn–53Cr cosmochronology. *Geochim. Cosmochim. Acta* **175**, 20–35.

Qin L., Alexander C. M. D., Carlson R. W., Horan M. F. and Yokoyama T. (2010) Contributors to chromium isotope variation of meteorites. *Geochim. Cosmochim. Acta* **74**, 1122–1145.

Qin L., Xia J., Carlson R. and Zhang Q. (2015) Chromium stable isotope composition of meteorites. *Lunar and Planetary Science Conference*.

Rhodes J. M., Huang S., Frey F. A., Pringle M. and Xu G. (2012) Compositional diversity of Mauna Kea shield lavas recovered by the Hawaii Scientific Drilling Project: Inferences on source lithology, magma supply, and the role of multiple volcanoes. *Geochem. Geophys. Geosyst.*, 13.

Rhodes J. and Vollinger M. (2004) Composition of basaltic lavas sampled by phase-2 of the Hawaii Scientific Drilling Project: Geochemical stratigraphy and magma types. *Geochem. Geophys. Geosyst.* **5**.

Roden M., Trull T., Hart S. and Frey F. (1994) New He, Nd, Pb, and Sr isotopic constraints on the constitution of the Hawaiian plume: results from Koolau Volcano, Oahu, Hawaii, USA. *Geochim. Cosmochim. Acta* **58**, 1431–1440.

Roeder P., Gofton E. and Thornber C. (2006) Cotectic proportions of olivine and spinel in olivine-tholeiitic basalt and evaluation of pre-eruptive processes. *J. Petrol.* **47**, 883–900.

Roeder P. and Reynolds I. (1991) Crystallization of chromite and chromium solubility in basaltic melts. *J. Petrol.* **32**, 909–934.

Roeder P. L., Poustovetov A. and Oskarsson N. (2001) Growth forms and composition of chromian spinel in MORB magma: diffusion-controlled crystallization of chromian spinel. *Can. Mineral.* **39**, 397–416.

Schoenberg R., Merdian A., Holmden C., Kleinhanns I. C., Haßler K., Wille M. and Reitter E. (2016) The stable Cr isotopic compositions of chondrites and silicate planetary reservoirs. *Geochim. Cosmochim. Acta* **183**, 14–30.

Schoenberg R., Zink S., Staubwasser M. and Von Blanckenburg F. (2008) The stable Cr isotope inventory of solid Earth reservoirs determined by double spike MC-ICP-MS. *Chem. Geol.* **249**, 294–306.

Scowen P., Roeder P. and Helz R. (1991) Reequilibration of chromite within Kilauea Iki lava lake, Hawaii. *Contrib. Mineral. Petrol.* **107**, 8–20.

Shen J., Liu J., Qin L., Wang S. J., Li S., Xia J., Ke S. and Yang J. (2015) Chromium isotope signature during continental crust subduction recorded in metamorphic rocks. *Geochem. Geophys. Geosyst.* **16**, 3840–3854.

Shen J., Qin L., Fang Z., Zhang Y., Liu J., Liu W., Wang F., Xiao Y., Yu H. and Wei S. (2018) High-temperature inter-mineral Cr isotope fractionation: A comparison of ionic model predictions and experimental investigations of mantle xenoliths from the North China Craton. *Earth Planet. Sci. Lett.* **499**, 278–290.

Silva I. G. N., Weis D. and Scoates J. S. (2013) Isotopic systematics of the early Mauna Kea shield phase and insight into the deep mantle beneath the Pacific Ocean. *Geochem. Geophys. Geosyst.* **14**, 659–676.

Sobolev A. V., Hofmann A. W., Kuzmin D. V., Yaxley G. M., Arndt N. T., Chung S.-L., Danyushevsky L. V., Elliott T., Frey F. A. and Garcia M. O. (2007) The amount of recycled crust in sources of mantle-derived melts. *Science* **316**, 412–417.

Sobolev A. V., Hofmann A. W., Sobolev S. V. and Nikogosian I. K. (2005) An olivine-free mantle source of Hawaiian shield basalts. *Nature* **434**, 590.

Sossi P. A., Foden J. D. and Halverson G. P. (2012) Redox-controlled iron isotope fractionation during magmatic differentiation: an example from the Red Hill intrusion. *S. Tasmania. Contrib. Mineral. Petrol.* **164**, 757–772.

Sossi P. A., Moynier F. and Van Zuilen K. (2018) Volatile loss following cooling and accretion of the Moon revealed by chromium isotopes. *Proc. Natl. Acad. Sci.* **115**, 10920–10925.

Sossi P. A. and O'Neill H. S. C. (2017) The effect of bonding environment on iron isotope fractionation between minerals at high temperature. *Geochim. Cosmochim. Acta* **196**, 121–143.

Sutton S., Jones K., Gordon B., Rivers M., Bajt S. and Smith J. (1993) Reduced chromium in olivine grains from lunar basalt 15555: X-ray absorption near edge structure (XANES). *Geochim. Cosmochim. Acta* **57**, 461–468.

Teng F.-Z., Dauphas N., Helz R. T., Gao S. and Huang S. (2011) Diffusion-driven magnesium and iron isotope fractionation in Hawaiian olivine. *Earth Planet. Sci. Lett.* **308**, 317–324.

Teng F.-Z., Wadhwa M. and Helz R. T. (2007) Investigation of magnesium isotope fractionation during basalt differentiation: Implications for a chondritic composition of the terrestrial mantle. *Earth Planet. Sci. Lett.* **261**, 84–92.

Teng F. Z., Dauphas N. and Helz R. T. (2008) Iron Isotope Fractionation During Magmatic Differentiation in Kilauea Iki Lava Lake. *Science* **320**, 1620–1622.

Teng F. Z., Dauphas N., Huang S. and Marty B. (2013) Iron isotopic systematics of oceanic basalts. *Geochim. Cosmochim. Acta* **107**, 12–26.

Trinquier A., Birck J.-L. and Allègre C. J. (2008) High-precision analysis of chromium isotopes in terrestrial and meteorite samples by thermal ionization mass spectrometry. *J. Anal. At. Spectrom.* **23**, 1565–1574.

Wadhwa M. (2008) Redox conditions on small bodies, the Moon and Mars. *Rev. Mineral. Geochem.* **68**, 493–510.

Wang X., Planavsky N. J., Reinhard C. T., Zou H., Ague J. J., Wu Y., Gill B. C., Schwarzenbach E. M. and Peucker-Ehrenbrink B. (2016) Chromium isotope fractionation during subduction-related metamorphism, black shale weathering, and hydrothermal alteration. *Chem. Geol.* **423**, 19–33.

Xia J., Qin L., Shen J., Carlson R. W., Ionov D. A. and Mock T. D. (2017) Chromium isotope heterogeneity in the mantle. *Earth Planet. Sci. Lett.* **464**, 103–115.

Young E. D., Manning C. E., Schauble E. A., Shahar A., Macris C. A., Lazar C. and Jordan M. (2015) High-temperature equilibrium isotope fractionation of non-traditional stable isotopes: Experiments, theory, and applications. *Chem. Geol.* **395**, 176–195.

Zhang H., Wang Y., He Y., Teng F. Z., Jacobsen S. B., Helz R. T., Marsh B. D. and Huang S. (2018) No measurable calcium isotopic fractionation during crystallization of Kilauea Iki lava lake. *Geochem. Geophys. Geosyst.* **19**, 3128–3139.

Zhu K., Sossi P. A., Siebert J. and Moynier F. (2019) Tracking the volatile and magmatic history of Vesta from chromium stable isotope variations in eucrite and diogenite meteorites. *Geochim. Cosmochim. Acta* **266**, 598–610.

Associate editor: Fang-Zhen Teng